CrossMark

JM PAPERS

Law of bounded dissipation and its consequences in turbulent wall flows

Xi Chen[1],† and Katepalli R. Sreenivasan[2]

[1]Key Laboratory of Fluid Mechanics of Ministry of Education, Beihang University (Beijing University of Aeronautics and Astronautics), Beijing, PR China

[2]Tandon School of Engineering, Courant Institute of Mathematical Sciences, Department of Physics, New York University, New York, USA

The dominant paradigm in turbulent wall flows is that the mean velocity near the wall, when scaled on wall variables, is independent of the friction Reynolds number Re_τ. This paradigm faces challenges when applied to fluctuations but has received serious attention only recently. Here, by extending our earlier work (Chen & Sreenivasan, *J. Fluid Mech.*, vol. 908, 2021, p. R3) we present a promising perspective, and support it with data, that fluctuations displaying non-zero wall values, or near-wall peaks, are bounded for large values of Re_τ, owing to the natural constraint that the dissipation rate is bounded. Specifically, $\Phi_\infty - \Phi = C_\Phi\, Re_\tau^{-1/4}$, where Φ represents the maximum value of any of the following quantities: energy dissipation rate, turbulent diffusion, fluctuations of pressure, streamwise and spanwise velocities, squares of vorticity components, and the wall values of pressure and shear stresses; the subscript ∞ denotes the bounded asymptotic value of Φ, and the coefficient C_Φ depends on Φ but not on Re_τ. Moreover, there exists a scaling law for the maximum value in the wall-normal direction of high-order moments, of the form $\langle \varphi^{2q} \rangle_{max}^{1/q} = \alpha_q - \beta_q Re_\tau^{-1/4}$, where φ represents the streamwise or spanwise velocity fluctuation, and α_q and β_q are independent of Re_τ. Excellent agreement with available data is observed. A stochastic process for which the random variable has the form just mentioned, referred to here as the 'linear q-norm Gaussian', is proposed to explain the observed linear dependence of α_q on q.

Key words: turbulence theory, turbulent boundary layers, pipe flow boundary layer

1. Introduction

Turbulent flows past solid boundaries are ubiquitous. Working against molecular viscosity, ν, the fluid motion exerts large shear stress on the wall and dissipates more energy at

† Email address for correspondence: chenxi97@outlook.com

the wall than further away. The process is accompanied by the generation of intense turbulent fluctuations at or near the wall. The variation of the peak intensities with the flow Reynolds number is fundamental to the understanding of the ultimate statistical state of wall turbulence. It may also be of practical interest as the peak intensities could be surrogates for the turbulent energy generated by airborne and marine vehicles, and thus for their energy consumption.

Ever since a theory for turbulent shear flows began to develop, the dominant paradigm has been that the flow near the wall scales solely on ν and the wall shear stress, τ_w. This theme has been remarkably successful for the mean velocity, as evidenced by the law of the wall (for recent discussions, see Monkewitz, Chauhan & Nagib 2007; Nagib, Chauhan & Monkewitz 2007; Marusic *et al.* 2010; Smits, McKeon & Marusic 2011). Similar expectations for turbulent intensities are assumed in engineering models (such as the $k - \omega$ and $k - \varepsilon$ models reported in Wilcox 2006). In practice, this means that turbulence fluctuations, after suitable normalization by the wall stress and viscosity, would be invariant with respect to the friction Reynolds number $Re_\tau = u_\tau \delta / \nu$, where $u_\tau \equiv \tau_w^{1/2}$ (with density absorbed) is the friction velocity and δ is the flow thickness. Nevertheless, as found in direct numerical simulations (DNS) (Spalart 1988; Moser, Kim & Mansour 1999; Skote 2001; Iwamoto, Suzuki & Kasagi 2002; Hoyas & Jimenez 2006; Orlandi & Leonardi 2007; Wu & Moin 2008; Schlatter *et al.* 2009; Sillero, Jimenez & Moser 2013; Ahn *et al.* 2015; Lee & Moser 2015; Yamamoto & Tsuji 2018) and in laboratory experiments (EXP) (Sreenivasan 1989; DeGraaff & Eaton 2000; Örlü 2009; Hultmark *et al.* 2012; Vincenti *et al.* 2013; Marusic *et al.* 2015; Vallikivi, Ganapathisubramani & Smits 2015; Willert *et al.* 2017; Samie *et al.* 2018), wall-normalized fluctuating quantities increase with Re_τ. These include (almost) all quantities with wall values that are non-zero or display near-wall peaks – in particular, in the wall components of energy dissipation (ε_{x-w}^+ and ε_{z-w}^+), diffusion ($\mathcal{D}_{x-w}^+$ and $\mathcal{D}_{z-w}^+$), root-mean-square (r.m.s.) vorticity ($\omega_{x-w}'^+$ and $\omega_{z-w}'^+$), and r.m.s. wall shear stress ($\tau_{x-w}'^+$ and $\tau_{z-w}'^+$) and pressure ($p_w'^+$), absorbing the fluid density in the definition of pressure; the list also includes the near-wall intensity peaks of velocities ($u_p'^+$ occurring at $y^+ \approx 15$, and $w_p'^+$ occurring at $y^+ \approx 45$) and pressure fluctuation ($p_p'^+$ occurring at $y^+ \approx 30$). We adopt the standard convention that a superscript $+$ indicates normalization by u_τ and ν, and a superscript prime represents the r.m.s. fluctuation. Subscript w represents the wall, p the peak value near the wall, u, v, w fluctuation velocities in the streamwise (x), wall-normal (y) and spanwise/azimuthal (z) directions; where two letters are used as subscripts, they indicate wall (w) values and the direction x, y or z. The increase of these quantities with Re_τ cannot be explained away by stating that the flow has not reached a fully developed state; so they pose a challenge for the classical wall-scaling for turbulent fluctuations, particularly for high-*Re* predictions. Our goal is to present a unified view of their variations with the flow Reynolds number, which is absent in the descriptions of wall turbulence so far.

This quest has been around at least since Sreenivasan (1989) and could probably be dated back to Bradshaw (1967) who addressed Townsend (1956)'s hypothesis of 'active' and 'inactive' motion. Since then, there exist: the mixed scaling argument by DeGraaff & Eaton (2000) and the inner–outer interaction by Marusic, Baars & Hutchins (2017) to explain the growth of $u_p'^{+2}$; the additive multifractal model by Yang & Lozano-Durán (2017) for the growth of streamwise wall shear stress $\tau_{x-w}'^+$, addressed also by Schlatter & Örlü (2010) and Tardu (2017); the growth of spanwise wall shear stress $\tau_{z-w}'^+$ or wall dissipation ε_{z-w}^+ by Diaz-Daniel, Laizet & Vassilicos (2017), also via the mixed scaling argument; the k^{-1} spectrum by Klewicki, Priyadarshana & Metzger (2008); and the

overlap region argument by Panton, Lee & Moser (2017) for the $p_w'^+$ growth (see also Bradshaw 1967). Moreover, Meneveau & Marusic (2013) extended the attached eddy model to examine the Re_τ-dependence of u'^+ moments in turbulent boundary layer (TBL) flows. All these works positing a logarithmic growth in Re_τ indicate the failure of the wall scaling for turbulent fluctuations because they grow without bound for asymptotically large Re_τ.

Recently, Chen & Sreenivasan (2021) (hereafter CS) reexamined this issue and showed that the near-wall growth of u'^{+2} is ultimately constrained by the finite value of the wall dissipation rate, itself bounded by the maximum turbulent production rate of 1/4 in wall units. Following the CS picture, Hultmark & Smits (2021) and later Smits *et al.* (2021) presented a good data collapse of near-wall profiles of velocity intensity for different Re_τ using the wall shear stress fluctuation $\tau_{x-w}'^{+2}$ (which equals the wall dissipation rate ε_{x-w}^+) as the scaling variable. The use of $Re_\tau^{-1/4}$ as the scaling factor has been adopted further in an important paper by Monkewitz (2021) as the small expansion parameter to develop composite models for near-wall u'^{+2} profiles. Indeed, models for finite-Reynolds-number effects are needed for the development of the subject that is generally dominated by experimental and numerical data. Also in the recent pipe DNS by Pirozzoli *et al.* (2021), the $Re_\tau^{-1/4}$ scaling is validated for ε_{x-w}^+, even though the authors state that the saturation of $u_p'^{+2}$ remains open due to limited Re_τ domain (up to 6000). Overall, taking the CS considerations as essentially correct, it seems worth exploring whether other near-wall fluctuations exhibit similar boundedness. If so, the results would support classical wall scaling and indicate a bounded near-wall turbulence for asymptotically large Re_τ, which would constitute an important conclusion.

Section 2 contains the bulk of comparisons with experimental data on single-point second-order fluctuation variables mentioned above, while § 3 contains comparisons with higher-order moments. Section 4 describes a new statistical model of a process that describes the observations of § 3. Section 5 is devoted to a discussion of the quality and limitations of the present data on which high-Reynolds-number behaviours are inferred, and § 6 summarizes the results and provides a context for them.

2. Bounded dissipation and the $Re_\tau^{-1/4}$ defect power law

We present a broad explanation for the growth of quantities just mentioned, on the basis of the law for bounded wall dissipation advanced by CS. We recall that the latter is expressed as

$$\varepsilon_{x-w,\infty}^+ - \varepsilon_{x-w}^+ = C_\varepsilon Re_\tau^{-1/4}, \tag{2.1}$$

where $\varepsilon_x = \nu\langle|\nabla u|^2\rangle$ is the streamwise wall dissipation ($\langle\cdot\rangle$ denotes average), C_ε is a constant independent of the Reynolds number, and $\varepsilon_{x-w,\infty}$ is the asymptote as $Re_\tau \to \infty$ of ε_{x-w}, which is the wall value of ε_x. After normalization using u_τ^4/ν, $\varepsilon_{x-w,\infty}^+$ is thought to be bounded by 1/4, which is the constraint imposed by the exact maximum production. CS verified this scaling by comparisons with available data, and also provided the following physical rationale for (2.1). What controls the turbulence peak values at any Reynolds number is the peak energy dissipation, which equals the maximum production only at infinitely large Reynolds number; and at any finite Reynolds number, it is the departure of the dissipation rate from its limiting value that determines the finite Reynolds number dependence. Specifically, the peak dissipation falls short of the peak energy production of 1/4 at finite Reynolds number by transmitting outwards in the amount $\varepsilon_d = u_\tau^3/\eta_0$,

Quantity Φ	$\Phi_\infty^{(CH)}$	$\Phi_\infty^{(Pipe)}$	$\Phi_\infty^{(TBL)}$	$C_\Phi^{(CH)}$	$C_\Phi^{(Pipe)}$	$C_\Phi^{(TBL)}$
$\varepsilon_{x-w}(=\mathcal{D}_{x-w}=\tau_{x-w}^{'2}=\omega_{z-w}^{'2})$	1/4	1/4	0.23	0.42	0.45	0.29
$\varepsilon_{z-w}(=\mathcal{D}_{z-w}=\tau_{z-w}^{'2}=\omega_{x-w}^{'2})$	0.13	0.13	0.13	0.31	0.31	0.25
p_w'	4.4	4.4	4.5	10.5	10.5	9.7
p_p'	4.84	4.84	4.95	10.5	10.5	9.7
$u_p'^2$	11.5	11.5	11.5	19.3	19.3	19.3
$w_p'^2$	3.9	3.9	4.1	10	10	10

Table 1. Parameters in (2.2), i.e. $\Phi = \Phi_\infty - C_\Phi Re_\tau^{-1/4}$, for different fluctuations after normalization in viscous units. Superscripts 'CH', 'Pipe' and 'TBL' represent channel, pipe and boundary layer flows, respectively.

where η_0 is the outer flow Kolmogorov length scale, and hence $\varepsilon_d^+ = \varepsilon_d/(u_\tau^4/\nu) \sim Re_\tau^{-1/4}$ leading to (2.1). For more details of the argument, one may consult CS.

A natural generalization of the above result (2.1) is

$$\Phi_\infty - \Phi = C_\Phi\, Re_\tau^{-1/4}, \tag{2.2}$$

where Φ is any of the quantities ε_{x-w}^+, ε_{z-w}^+, $\mathcal{D}_{x-w}^+$, $\mathcal{D}_{z-w}^+$, $\omega_{z-w}^{'+2}$, $\omega_{x-w}^{'+2}$, $\tau_{x-w}^{'+2}$, $\tau_{z-w}^{'+2}$, $p_w'^+$, $p_p'^+$, $u_p'^{+2}$ and $w_p'^{+2}$; the subscript ∞ denotes bounded asymptotic values, and the coefficient C_Φ depends on the quantity Φ in question but not on the Reynolds number. We also note that $\varepsilon_{x-w}^+ = \tau_{x-w}^{'+2} = \omega_{z-w}^{'+2} = \langle(\partial u^+/\partial y^+)^2\rangle_w$ and $\varepsilon_{z-w}^+ = \tau_{z-w}^{'+2} = \omega_{x-w}^{'+2} = \langle(\partial w^+/\partial y^+)^2\rangle_w$ due to the no-slip wall condition (i.e. $\nabla u = \partial_y u$ and $\nabla w = \partial_y w$ at the wall), while $\mathcal{D}_{x-w}^+ = \varepsilon_{x-w}^+$ and $\mathcal{D}_{z-w}^+ = \varepsilon_{z-w}^+$ because of the Reynolds stress balances at the wall.

The generalization (2.2) is indeed conceivable because dissipation structures of ε_x are highly correlated with u-streaks and hence associated closely with near-wall streamwise vortices, which are organized in a self-sustaining cycle. The latter structures would generate dissipation in the spanwise direction, induce w-streaks and cause inhomogeneous pressure distributions. Thus the near-wall quantities should all be treated in some uniform manner, which is what is proposed here. Table 1 summarizes the essential data on almost all the single-point second-order turbulent statistics with non-zero wall values or near-wall peaks, each examined separately as follows.

Figure 1 shows comparisons of wall dissipation rates, with the top panels showing the streamwise component and the bottom panels the spanwise component; also shown are the logarithmic growth rates discussed by different authors in the literature. Figure 2 shows similar comparisons for the peak pressure fluctuation (top panels) and the wall pressure fluctuation (bottom panels). Figure 3 shows comparisons of u_p' (top panels) and w_p' (bottom panels). In all these plots, the left-hand panels are for channel and pipe, while the right-hand panels are for TBL. For simplicity of notation, the superscript $+$ is omitted from here on unless otherwise specified. The agreement between data and (2.2) is excellent. A quantitative observation for the three flows is that the dissipation component in the z direction is about half of that in the x direction at the same Re_τ; and wall pressure is slightly smaller by 0.4 than the peak pressure, with both pressures of the same order as $u_p'^2$ and $w_p'^2$.

The parameters in (2.2) for the six independent quantities, shown in figures 1–3, form the basis of table 1. Data in figures 1–3 are from the original sources of DNS and
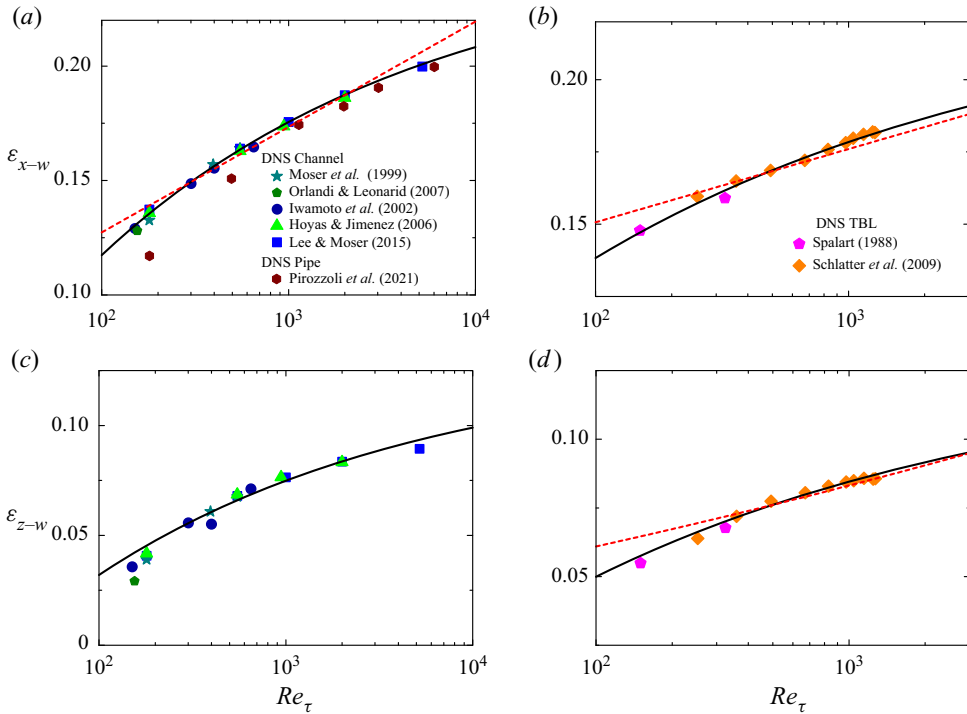
933 A20-4

Figure 1. Re_τ-variations of wall dissipation rates after normalization in viscous units. Streamwise velocity component ε_{x-w} – equivalently, the fluctuation intensities of streamwise wall shear stress τ'^2_{x-w} and spanwise wall vorticity ω'^2_{z-w} – in channel and pipe flows (*a*) and in TBL flows (*b*). Spanwise velocity component ε_{z-w} – also the intensities of spanwise wall shear stress τ'^2_{z-w} and streamwise wall vorticity ω'^2_{x-w} – in channel and pipe flows (*c*) and in TBL flows (*d*). Solid lines are predictions for channel (*a,c*) and TBL (*b,d*) by using (2.2), with the parameters summarized in table 1. Dashed lines indicate logarithmic growths in the literature, i.e. $\varepsilon_{x-w} = 0.02 \ln(Re_\tau) + 0.035$ by Tardu (2017) in (*a*), $\varepsilon_{x-w} = 0.011 \ln(Re_\tau) + 0.10$ by Yang & Lozano-Durán (2017) in (*b*), and $\varepsilon_{z-w} = [0.018 \ln(Re_\tau) + 0.164]^2$ by Diaz-Daniel *et al.* (2017) in (*d*), whilst no logarithmic growth for ε_{z-w} in channel/pipe is found in public and hence is absent in (*c*). Solid symbols are DNS data of channels: star, Moser *et al.* (1999); pentagon, Orlandi & Leonardi (2007); circle, Iwamoto *et al.* (2002); upward triangle, Hoyas & Jimenez (2006); square, Lee & Moser (2015). For pipes: hexagon, Pirozzoli *et al.* (2021). For TBLs: pentagon, Spalart (1988); diamond, Schlatter *et al.* (2009). Here and elsewhere, for brevity, symbols are explained in figure legends when they appear for the first time.

EXP measurements (see legends); all available data are included as long as meaningful definition of the peak and wall values are possible. Note that $\mathcal{D}_{x-w}$ and $\mathcal{D}_{z-w}$ would provide another two independent checks of (2.2) but they are not explicitly compared here as their published data are sparser than those in figures 1–3. Moreover, τ'_{x-w}, τ'_{z-w}, ω'_{z-w} and ω'_{x-w} can be obtained through definitions from mean quantities in table 1, so there is no need to show them separately.

The noteworthy points that emerge from these extensive comparisons are as follows.

(1) The proportionality coefficient C_Φ varies only modestly when the flow direction changes from x to z or from channel and pipe to TBL, implying that essentially the same mechanism applies for all flows.

(2) DNS data of pipe follow, overall, the channel data, except for ε_{x-w}, for which C_Φ differs slightly.
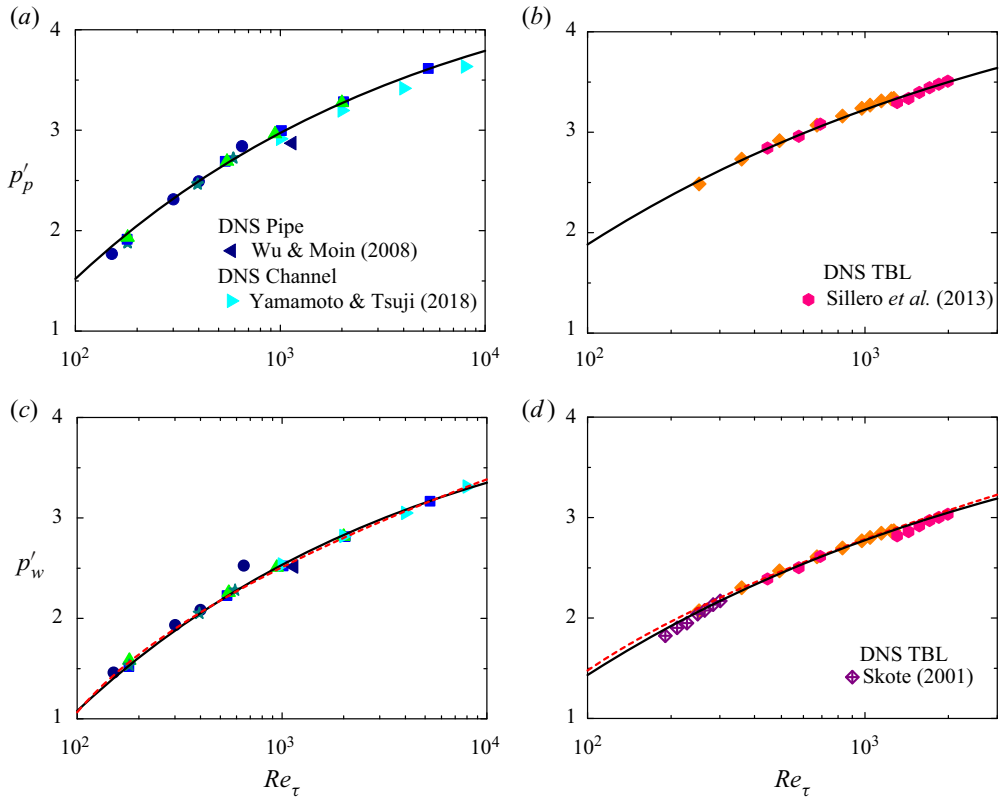
Figure 2. Plots of intensities of peak pressure (*a,b*) and wall pressure (*c,d*), similar to figure 1. Again, solid lines are fits to (2.2); dashed lines indicate logarithmic growths for wall pressure by Panton *et al.* (2017), i.e. $p_w'^2 = 2.24 \ln(Re_\tau) - 9.18$ in (*c*) for channels and pipes, and $p_w'^2 = 2.42 \ln(Re_\tau) - 8.96$ in (*d*) for TBLs. Newly included solid symbols are DNS data for pipes (leftward triangle, Wu & Moin (2008)), for channels (rightward triangle, Yamamoto & Tsuji (2018)) and for TBLs (hexagon, Sillero *et al.* (2013); diamond with cross, Skote (2001)). Other symbols are the same as in figure 1.

(3) The fitted Φ_∞ for each mean quantity seems to be universal among channel, pipe and TBL flows, except for differences of the order of 8 % for ε_{x-w}, 2 % for p_p' and p_w', and 5 % for w_p', which may be attributed to the uncertainty in transition histories – although we concede the possibility that pipes and channels and TBLs may need to be considered separately if the accuracy of the data improves over time.

(4) The fitted $\Phi_\infty = 0.23$ for ε_{x-w} in TBLs is very close to our theoretical value $1/4$ (validated for ε_{x-w} in channels and pipes), which bounds the maximum turbulent production.

(5) The atmospheric boundary layer measurement over the Salt Lake data of p' at the wall is reported to be approximately 4.98 at $Re_\tau = 10^6$ by Klewicki *et al.* (2008), 10 % higher than our predicted asymptotic wall pressure $p_w' = 4.5$ but agreeing closely with the peak pressure $p_p' = 4.95$ (located at $y^+ = 30$ in viscous units, very close to the wall).

(6) The Salt Lake data of $u_p'^2$ are reported to give around 13.4 with 20 % uncertainty at $Re_\tau = 10^6$ (Metzger & Klewicki 2001), overlapping with our estimate of $u_p'^2 = 11.5$
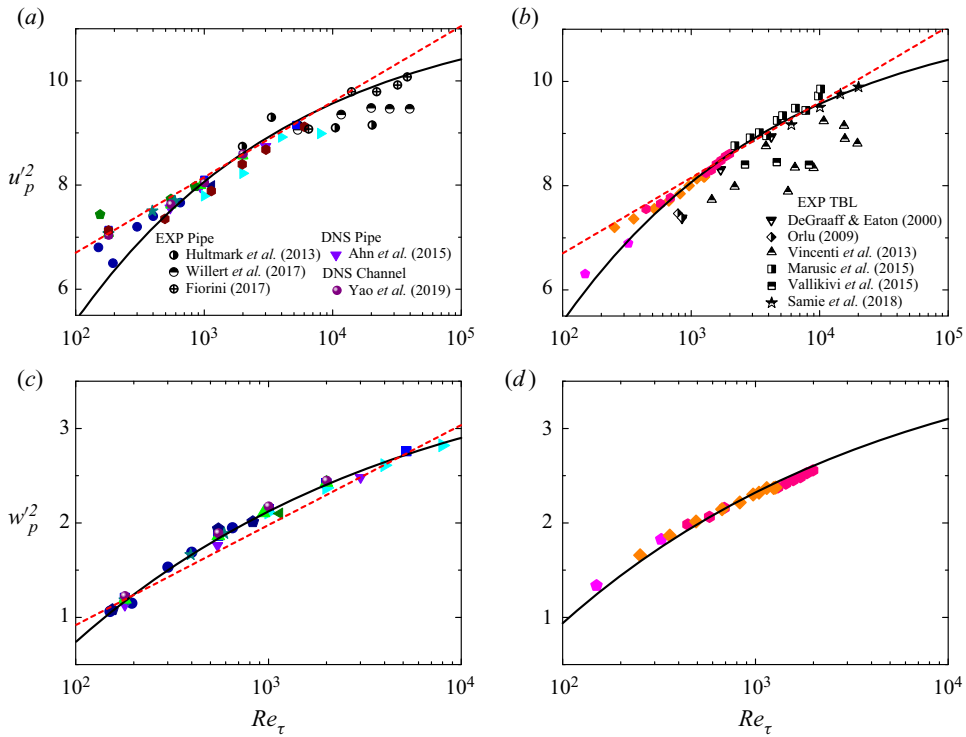
Figure 3. The Re_τ-variations of peak turbulence intensities. Streamwise intensity u'^2_p in channel and pipe (*a*), and in TBL (*b*). Spanwise intensity w'^2_p in channel and pipe (*c*), and in TBL (*d*). Newly included data are: EXP pipes of Princeton by Hultmark *et al.* (2012), of CICLoPE by Willert *et al.* (2017) based on PIV measurement, and by Fiorini (2017) with hot-wire data corrected; DNS data of pipes by Ahn *et al.* (2015) and of channels by Yao, Chen & Hussain (2019); EXP data of TBL by DeGraaff & Eaton (2000), Örlü (2009), Vincenti *et al.* (2013), Marusic *et al.* (2015), Vallikivi *et al.* (2015) and Samie *et al.* (2018); see figure legends for the corresponding symbols. Solid lines are fit to (2.2), whose parameters are summarized in table 1. Dashed lines indicate $u'^2_p = 0.63 \ln(Re_\tau) + 3.8$ by Marusic *et al.* (2017), and $w'^2_p = 0.46 \ln(Re_\tau) - 1.2$ adopted by us for reference, both of which arise from the Gaussian-logarithmic model for high-order moments, as discussed in the text and shown in figures 4 and 5.

for asymptotically high Re_τ. Thus, from these items (1)–(6), one may regard (2.2) as validated by a large volume of data.

Special attention is drawn to u'^2_p shown in the top panels of figure 3. In contrast to other quantities, there are notable departures between data and (2.2) for Re_τ less than 500; however, the agreement improves towards higher Re_τ. By adjusting $\Phi_\infty = 10.5$ and $C_\Phi = 12.7$, better agreement can be achieved for smaller Re_τ, but these new constants are not as good as the current ones for high Re_τ data. A similar situation is also present in the competing log variation. For example, the log law slope is reported as 0.63 by Marusic *et al.* (2017) for the Re_τ fitting range between 500 and 20 000 (shown in the top panels of figure 3); however, considering Re_τ between 1000 and 5000 only, Lee & Moser (2015) found the slope as 0.642 for channel and, very recently, Pirozzoli *et al.* (2021) found the slope to be 0.612 by choosing a Re_τ range between 180 and 6000 for pipes. Therefore, taking a conservative stance, one cannot yet draw a solid conclusion on the log law slope, nor on the superiority of the competitive log law and (2.2) regarding the
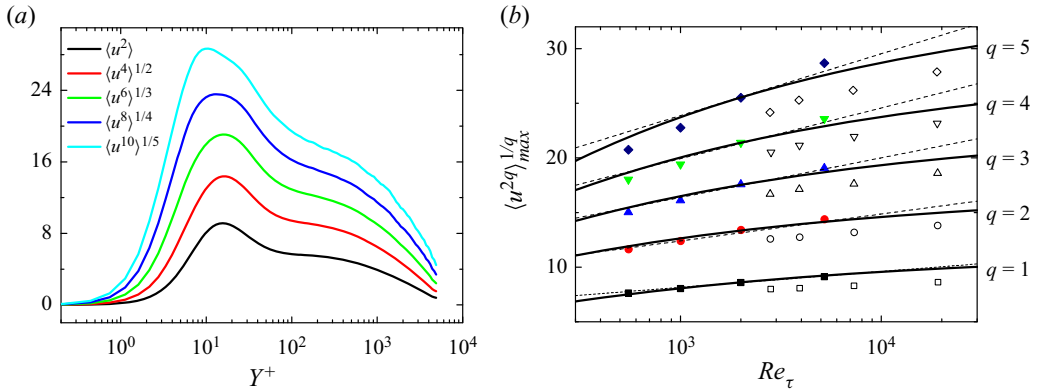
Figure 4. (*a*) Wall-normal dependence of *u*-moments at $Re_\tau = 5200$ in the DNS data of Lee & Moser (2015). (*b*) Re_τ variations of the maximum *u* moments near the wall. In (*b*): solid symbols represent the DNS channel data of Lee & Moser (2015); open symbols are EXP TBL data by Hutchins *et al.* (2009), extracted from Meneveau & Marusic (2013); and solid lines come from (3.1) in CS, compared with dashed lines from (3.2) and (3.3) by Meneveau & Marusic (2013).

'correct' $u_p'^2$ scaling. Currently, it is unknown whether the departure between the data and different scaling proposals at small Reynolds number is due to transition history, or a physical transition in scaling at a critical $Re_\tau \approx 500$. To track this subtle issue, quality data for a one high-quality flow covering both small and large Reynolds number with fine resolution is needed. Another issue is whether channel, pipe and TBL have the same Re_τ scaling for $u_p'^2$; this remains unclear, recalling that Samie *et al.* (2018) found the log law slope for TBL as 0.646, larger than all the values obtained for channel and pipe flows.

3. Scaling of velocity fluctuation moments near the wall

It is interesting to examine the scaling of high-order (even) moments of fluctuations, e.g. $\langle u^{2q} \rangle^{1/q}$ and $\langle w^{2q} \rangle^{1/q}$ for $q = 1$ to $q = 5$. Figure 4(*a*) shows the wall-normal profiles of fluctuation moments for *u* at $Re_\tau = 5200$; similarly, figure 5(*a*) plots moments of *w* for the same Re_τ. Near-wall peaks are observed for all these moments, which are obtained from the Johns Hopkins Turbulence Database and contain more than 5×10^6 velocity samples. On the basis of scaling considerations similar to those used before, we argue that the maximum values of moments would also be bounded as $Re_\tau \to \infty$, and that the finite-Re_τ dependence is the same 1/4 power. Accordingly, we write

$$\langle \varphi^{2q} \rangle_{max}^{1/q} = \alpha_q - \beta_q Re_\tau^{-1/4}, \tag{3.1}$$

where φ represents either *u* or *w* fluctuations, and α_q represents different asymptotes for different *q* when $Re_\tau \to \infty$; β_q is independent of Re_τ. Note that for $q = 1$, $\alpha_1 = \Phi_\infty$ and $\beta_1 = C_\Phi$ in (2.2).

We now consider peaks in various moments of the velocity fluctuations in streamwise directions. Figure 4(*b*) shows Re_τ-variations for the near-wall peaks of $\langle u^{2q} \rangle^{1/q}$ for $q = 1$ to $q = 5$. Solid lines denote the defect power law fitting by (3.1), where values of α_q, shown in figure 6(*a*), are of particular interest because they represent the asymptotic values of $\langle u^{2q} \rangle^{1/q}$. Similarly, figure 5(*b*) shows the Re_τ-variations of the maximum $\langle w^{2q} \rangle^{1/q}$, and the fit to the corresponding α_q is shown in figure 6(*b*). It is clear that (3.1) characterizes the
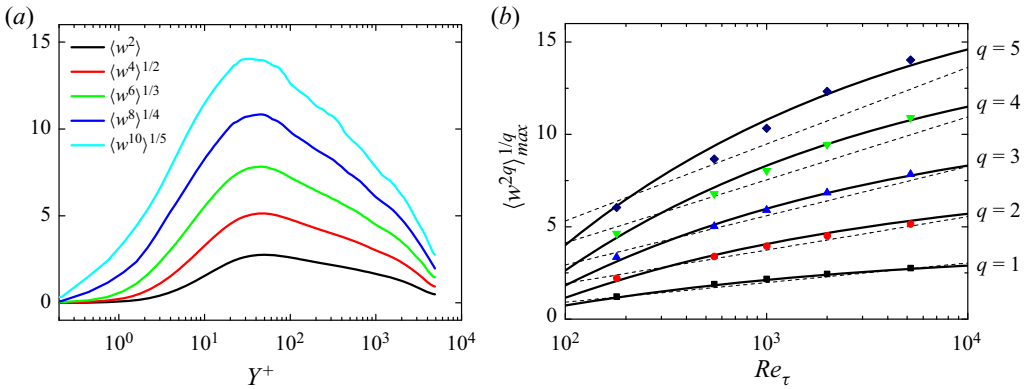
933 A20-8

Figure 5. (*a*) Wall-normal dependence of w-moments at $Re_\tau = 5200$. (*b*) Re_τ variations of the maximum w moments near the wall. Data are DNS channel by Lee & Moser (2015). In (*b*), solid lines come from (3.1) in CS, compared with dashed lines from (3.2) and (3.3) by Meneveau & Marusic (2013).
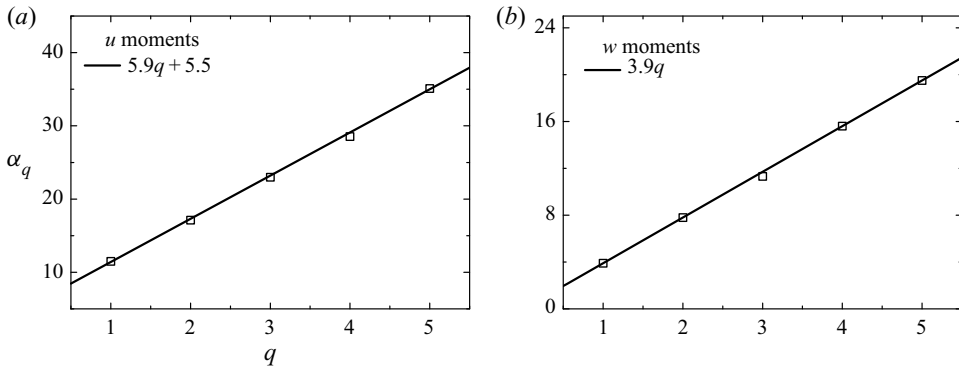

Figure 6. Variations with q of α_q for the moments of u (*a*) and w (*b*). Solid lines indicate linear dependence, explained in (4.10) and (4.11), given by the linear q-norm Gaussian process defined in (4.8).

data well, and α_q in both cases follows closely a linear relationship with q. Its underlying explanation will be presented in the next section.

Note for comparison that we include a Gaussian-logarithmic model by Meneveau & Marusic (2013) (hereafter referred to as MM) in figures 4(*b*) and 5(*b*), represented by the dashed lines. The MM model has the dependence

$$\langle \varphi^{2q} \rangle_{max}^{1/q} = A_q \ln(Re_\tau) + K_q, \tag{3.2}$$

together with the Gaussian random variable hypothesis for φ, yielding

$$A_q = A_1[(q-1)!!]^{1/q} \tag{3.3}$$

for the slopes, leaving the intercepts K_q arbitrary. Figure 4(*b*) shows that for u, (3.1) is comparable to the MM model; however, the difference becomes significant for w shown in figure 5(*b*). Overall, the MM model under-predicts the peaks of w moments. As noted by Meneveau & Marusic (2013), sub-Gaussian corrections may be needed to rectify this problem. However, this produces no improvement for $q = 1$ and does not change the inadequate agreement between data and the log proposal for $w_p'^2$; see figure 3(*c*) for the zoomed-in view. Taken together with plots of the preceding sections, the defect power law

(3.1) can be regarded as showing better agreement with data than the Gaussian-logarithmic growth (3.2).

4. Linear *q*-norm Gaussian process

In this section, we show that the linear *q*-dependence in figure 6 can result from a Gaussian random variable via an exponential transformation.

Let us first define the *q*-norm for a (random) variable ϕ as

$$\phi_q = \langle \phi^q \rangle^{1/q}, \tag{4.1}$$

where $\langle \cdot \rangle$ here represents the expectation value. If ϕ_q depends linearly on q, then it satisfies

$$\phi_q = \ln(\chi_q), \tag{4.2}$$

where χ_q is the *q*-norm of a log-normal variable χ, i.e. $\chi = e^\kappa$ with κ Gaussian distributed. This is demonstrated as follows.

Given κ, one readily obtains χ_q and hence ϕ_q. That is,

$$\chi_q = \langle \chi^q \rangle^{1/q} = \langle (e^\kappa)^q \rangle^{1/q} = \langle e^{q\kappa} \rangle^{1/q}, \tag{4.3}$$

$$\phi_q = \ln(\chi_q) = \ln(\langle e^{q\kappa} \rangle^{1/q}) = (1/q) \ln(\langle e^{q\kappa} \rangle). \tag{4.4}$$

Specifically, for a Gaussian variable κ with its mean μ and variance 2σ, one has

$$\ln(\langle e^{q\kappa} \rangle) = \mu q + \sigma q^2. \tag{4.5}$$

Substitution of (4.5) into (4.3) and (4.4) yields

$$\chi_q = [e^{\mu q + \sigma q^2}]^{1/q} = e^{\mu + \sigma q}, \tag{4.6}$$

$$\phi_q = \ln(\chi_q) = \mu + \sigma q. \tag{4.7}$$

We may refer to the random variable ϕ that has a linear *q*-norm (4.7) as the 'linear *q*-norm Gaussian' (LQNG) process generated by the Gaussian seed κ. The above procedure is summarized as follows:

$$\kappa \xrightarrow{E} \chi \xrightarrow{Q} \chi_q \xrightarrow{E^{-1}} \phi_q \xrightarrow{Q^{-1}} \phi; \quad \phi = Q^{-1}E^{-1}QE(\kappa). \tag{4.8}$$

Here, E and Q indicate operations of exponential transform and *q*-norm, respectively, which are non-commutable for random variables; and the superscript -1 indicates the inverse operation (supposing that ϕ is determined by its moments). In other words, the LQNG process satisfies the operator-reflection symmetry

$$E \circ Q(\phi) = Q \circ E(\kappa). \tag{4.9}$$

If ϕ and κ are non-random, then it is trivial that $\phi = \kappa$; instead, ϕ and κ here are random variables, and by assigning κ as a Gaussian variable, we obtain a linear dependence of ϕ_q on *q*.

For wall turbulence, the asymptotes for the near-wall peaks of $\langle u^{2q} \rangle^{1/q}$ and $\langle w^{2q} \rangle^{1/q}$ when $Re_\tau \to \infty$ are LQNG processes. That is, substituting $\phi = u^2$ in (4.7) gives

$$\alpha_{u,q} = \mu_u + \sigma_u q, \tag{4.10}$$

where $\mu_u \approx 5.5$ and $\sigma_u \approx 5.9$ according to figure 6(*a*). Similarly, substituting $\phi = w^2$ in (4.7) gives

$$\alpha_{w,q} = \mu_w + \sigma_w q, \tag{4.11}$$

where $\mu_w \approx 0$ and $\sigma_w \approx 3.9$ according to figure 6(*b*). The fact that $\mu_w \approx 0$ may reflect the absence of inactive motion in the *w*-component of the velocity.

933 A20-10

5. Discussion on data quality

Presently, the range of high-quality and accurate experimental data remains limited, particularly with respect to the verification of the scaling of u'_p and p'_p, and greater certainty will be possible only as better data become available. However, for w'_p and the wall dissipation, the two competing scaling proposals (i.e. 1/4 defect power law and the log law) already show notable differences in the Re_τ domain up to 10^4. Hence a cogent scaling verification for w'_p, ε_{x-w} and ε_{z-w} may already be on hand. In saying this, we assume that the present data on w'_p, ε_{x-w} and ε_{z-w} are of adequate accuracy, but the veracity of data is clearly the ultimate arbiter.

For the DNS data, a particular point is that different grid resolutions may influence statistics. As shown by Yang *et al.* (2021), to capture the extreme events of wall dissipation, very fine resolution is needed even at a moderate Re_τ, similar to the effect known for homogeneous and isotropic turbulence; see, for example, Yeung, Sreenivasan & Pope (2018). This brings up the question of data uncertainty, which, of course, is always deserving of attention; see Monkewitz (2021) for more discussions.

One may alternatively use indirect methods to estimate wall dissipation, e.g. $\varepsilon_{x-w} \approx (u'/U)^2$ (or $(u'/y)^2$) and $\varepsilon_{z-w} \approx (w'/U)^2$ (or $(w'/y)^2$) towards the wall. These near-wall Taylor expansions are technically correct for $y^+ \to 0$, but may introduce uncertainty in practice because of the finite grid. For example, figure 7(*a*) shows that the $(u'/U)^2$ values (half-open hexagons) at y^+ locations closest to the wall for the DNS data of Pirozzoli *et al.* (2021) are noticeably higher than the wall values of ε_{x-w} (solid hexagons). Such a difference could also be related to specific numerical schemes used in DNS. The difference is smaller and negligible for the data of Lee & Moser (2015) and of Hoyas & Jimenez (2006), both sources having used the spectral method; see half-open symbols in figure 7. Therefore the linear approximation by Taylor expansion agrees well in some simulations, but not in others. In any case, if one utilizes this extrapolation method to estimate ε_{x-w} in the absence of direct measurements of the wall dissipation, the open symbols in figure 7(*a*) result. One may even infer a log variation from these open symbols when the significant data scatter is ignored. However, for these same DNS data sets without direct measurements of ε_{z-w}, figure 7(*b*) shows $(w'/U)^2$ towards the wall following the 1/4 defect power law closely. Despite this agreement, all the issues on data uncertainty (including numerical schemes in DNS, hot-wire resolution in EXP, indirect estimation, etc.) need careful examination and are left for future examination.

Since the available Re_τ domain is not large, it is not surprising that other formula may fit data similarly well. For example, recalling the comparison for p'_w in figure 2, where the defect power law is indistinguishable from the square root of logarithmic growth, one may use $\Phi = \sqrt{A \ln Re_\tau + B}$ (where A and B are coefficients) to represent the wall dissipation rate. Similarly, if we change the scaling exponent of $-1/4$ and the proportional coefficient in (2.2) by $1/4 - \varepsilon_{x-w} \approx 0.38 Re_\tau^{-1/4.3}$ or $0.48 Re_\tau^{-1/3.7}$, both of them fit the data well. We should point out, however, that the rationale for these alternative proposals is absent.

So far, the above scaling relations are derived from consideration of how the wall dissipation departs from its presumed limit. It would be interesting to examine the relation between the wall dissipation defect and modulations imposed by the large-scale motions further away from the wall (Metzger & Klewicki 2001; Mathis, Hutchins & Marusic 2009). A phenomenological model such as the hierarchical random additive process (Yang & Lozano-Durán 2017) might be insightful in explaining how the wall-attached eddies are related to the various bounds proposed here. In this context, one may wonder why
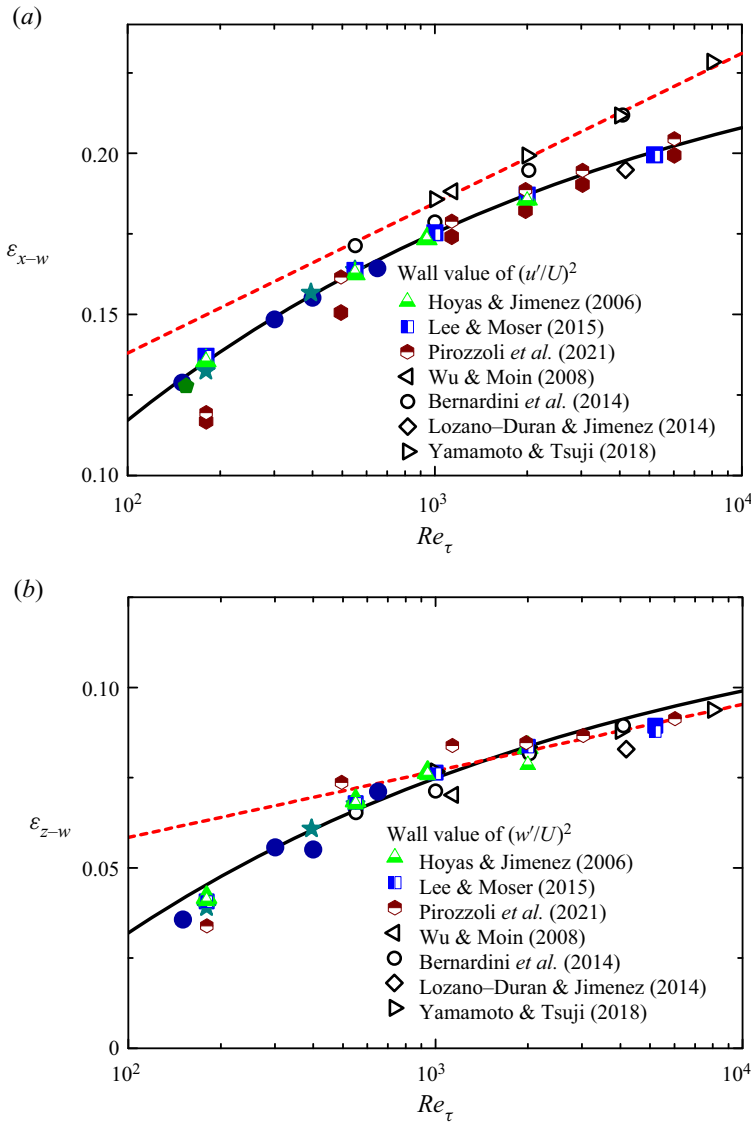
Figure 7. Same plots as figure 1(*a,c*), with newly added symbols (see legends) for wall values of $(u'/U)^2$ and $(w'/U)^2$ as approximations for ε_{x-w} (*a*) and ε_{z-w} (*b*), respectively. Solid lines are channel flow predictions according to (2.2), with the parameters summarized in table 1. Dashed lines indicate, for reference, the logarithmic growths, i.e. $0.0202 \ln(Re_\tau) + 0.045$ in (*a*) and $0.008 \ln(Re_\tau) + 0.0216$ in (*b*). Solid symbols represent wall dissipation, and are the same DNS data as in figure 1. Newly included half-open symbols are the DNS data. For channels: triangle, Hoyas & Jimenez (2006); square, Lee & Moser (2015). For pipes: hexagon, Pirozzoli *et al.* (2021). Newly included open symbols are from the DNS data (the wall dissipation rates being absent). For channels: circle, Bernardini, Pirozzoli & Orlandi (2014); diamond, Lozano-Durán & Jimenez (2014); rightward triangle, Yamamoto & Tsuji (2018). For pipes: leftward triangle, Wu & Moin (2008).

growing eddies lead to saturated wall fluctuations. A plausible answer is that the increasing contributions by these eddies are exactly accounted for by the normalization in u_τ, with the inactive motions becoming decreasingly influential. This is simply reminiscent of the Reynolds shear stress $\langle -uv \rangle$ and Reynolds normal stress $\langle vv \rangle$, referred to as the active

933 A20-12

motions by Townsend (1956), whose magnitudes are also thought to be bounded after scaling in wall units.

Additional comments may now be made regarding the scaling of active motions. In particular, the magnitudes of peak $\langle -uv \rangle$ and peak $\langle vv \rangle$ have been thought to obey – with theoretical support from the log law mean velocity (see Sreenivasan 1989; Pirozzoli *et al.* 2021; Smits *et al.* 2021) – the defect power law $1 - \langle -uv \rangle_p^+ \propto Re_\tau^{-1/2}$. However, a recent study by Chen, Hussain & She (2019) shows that $1 - \langle -uv \rangle_p^+$ exhibits different scaling transitions for channel/pipe on the one hand, and TBL flows on the other. Specifically, $1 - \langle -uv \rangle_p^+ \propto Re_\tau^{-2/3}$ for $Re_\tau < 1000$, and $1 - \langle -uv \rangle_p^+ \propto Re_\tau^{-1/2}$ for higher-Re_τ channel/pipe flows. The present paper focuses on wall values or near-wall fluctuations with invariant peak locations (e.g. for u', w' and p'), hence differing from the active motions (e.g. $\langle -uv \rangle$) extending infinitely far away from the wall (in y^+ units) as Re_τ increases. This is perhaps why they exhibit different defect power law exponents.

6. Conclusion

For the last three decades, considerable effort has been devoted to understanding the Re_τ growth of peak values of turbulent fluctuations, mostly based on the logarithmic form that shows an unbounded growth, thus indicating the breakdown of the wall scaling for turbulence fluctuations. While different arguments can, in fact, be invoked in those logarithmic descriptions, deviations from the log fits can be observed for ε_{x-w}, ε_{z-w} and w'_p in figures 1 and 3. The alternative (2.2) presented in this paper has shown that the averages of turbulent fluctuations – such as the intensities of wall shear stress, wall vorticity components, wall pressure, and intensity peaks of streamwise velocity, spanwise velocity and pressure, all of which possess non-zero wall values or near-wall peaks – follow a universal $Re_\tau^{-1/4}$ defect law. The underlying physics is that the maximum turbulent production provides a bounding constraint on the dissipation rate, and in turn on all near-wall quantities in the limit of infinite Reynolds number. What matters at any finite Reynolds number is the departure of the dissipation rate from its limiting value, as explained in CS. We have simply devised a way to describe the finite Re_τ correction as this asymptote is reached. The present proposal is validated against a large set of flow data.

The paper also extends the same argument to wall-normal peaks in high-order (even) moments of fluctuations. We have also produced a model that describes the variation of these higher moments of fluctuations. Together, the results support the classical wall scaling and indicate a bounded ultimate near-wall turbulence state. That is, moments of near-wall turbulence fluctuations, when suitably normalized by wall variables, attain constant values asymptotically at infinitely large Reynolds numbers. We believe that this is a significant conclusion.

Author ORCIDs.

Ⓓ Xi Chen https://orcid.org/0000-0002-4702-8735;

Ⓓ Katepalli R. Sreenivasan https://orcid.org/0000-0002-3943-6827.

REFERENCES

AHN, J.S., LEE, J.H., LEE, J., KANG, J.-H. & SUNG, H.J. 2015 Direct numerical simulation of a 30R long turbulent pipe flow at $Re_\tau = 3008$. *Phys. Fluids* **27**, 065110.

BERNARDINI, M., PIROZZOLI, S. & ORLANDI, P. 2014 Velocity statistics in turbulent channel flow up to $Re_\tau = 4000$. *J. Fluid Mech.* **742**, 171–191.

BRADSHAW, P. 1967 'Inactive' motion and pressure fluctuations in turbulent boundary layers. *J. Fluid Mech.* **30**, 241–258.

CHEN, X., HUSSAIN, F. & SHE, Z.S. 2019 Non-universal scaling transition of momentum cascade in wall turbulence. *J. Fluid Mech.* **871**, R2.

CHEN, X. & SREENIVASAN, K.R. 2021 Reynolds number scaling of the peak turbulence intensity in wall flows. *J. Fluid Mech.* **908**, R3.

DEGRAAFF, D.B. & EATON, J.K. 2000 Reynolds-number scaling of the flat plate turbulent boundary layer. *J. Fluid Mech.* **422**, 319–346.

DIAZ-DANIEL, C., LAIZET, S. & VASSILICOS, J.C. 2017 Wall shear stress fluctuations: mixed scaling and their effects on velocity fluctuations in a turbulent boundary layer. *Phys. Fluids* **29**, 055102.

FIORINI, T. 2017 Turbulent pipe flow – high resolution measurements in CICLoPE. PhD thesis, University of Bologna.

HOYAS, S. & JIMENEZ, J. 2006 Scaling of the velocity fluctuations in turbulent channels up to $Re_\tau = 2003$. *Phy. Fluids* **18**, 011702.

HULTMARK, M. & SMITS, A.J. 2021 Scaling turbulence in the near-wall region. arXiv:2103.01765v1.

HULTMARK, M., VALLIKIVI, M., BAILEY, S.C.C. & SMITS, A.J. 2012 Turbulent pipe flow at extreme Reynolds numbers. *Phys. Rev. Lett.* **108**, 094501.

HUTCHINS, N., NICKELS, T.B., MARUSIC, I. & CHONG, M.S. 2009 Hot-wire spatial resolution issues in wall-bounded turbulence. *J. Fluid Mech.* **635**, 103–136.

IWAMOTO, K., SUZUKI, Y. & KASAGI, N. 2002 Database of fully developed channel flow. *Tech. Rep.* ILR-0201, see http://www.thtlab.t.utokyo.ac.jp.

KLEWICKI, J.C., PRIYADARSHANA, P.J.A. & METZGER, M.M. 2008 Statistical structure of the fluctuating wall pressure and its in-plane gradients at high Reynolds number. *J. Fluid Mech.* **609**, 195–220.

LEE, M. & MOSER, R.D. 2015 Direct numerical simulation of turbulent channel flow up to $Re_\tau = 5200$. *J. Fluid Mech.* **774**, 395–415.

LOZANO-DURÁN, A. & JIMENEZ, J. 2014 Effect of the computational domain on direct simulations of turbulent channels up to $Re_\tau = 4200$. *Phys. Fluids* **26** (1), 011702.

MARUSIC, I., BAARS, W.J. & HUTCHINS, N. 2017 Scaling of the streamwise turbulence intensity in the context of inner-outer interactions in wall turbulence. *Phys. Rev. Fluids* **2**, 100502.

MARUSIC, I., CHAUHAN, K.A., KULANDAIVELU, V. & HUTCHINS, N. 2015 Evolution of zero-pressure-gradient boundary layers from different tripping conditions. *J. Fluid Mech.* **783**, 379–411.

MARUSIC, I., MCKEON, B.J., MONKEWITZ, P.A., NAGIB, H.M., SMITS, A.J. & SREENIVASAN, K.R. 2010 Wall-bounded turbulent flows at high Reynolds numbers: recent advances and key issues. *Phy. Fluids* **22**, 065103.

MATHIS, R., HUTCHINS, N. & MARUSIC, I. 2009 Large-scale amplitude modulation of the small-scale structures in turbulent boundary layers. *J. Fluid Mech.* **628**, 311–337.

MENEVEAU, C. & MARUSIC, I. 2013 Generalized logarithmic law for high-order moments in turbulent boundary layers. *J. Fluid Mech.* **719**, R1.

METZGER, M.M. & KLEWICKI, J. 2001 A comparative study of near-wall turbulence in high and low Reynolds number boundary layers. *Phys. Fluids* **13**, 692–701.

MONKEWITZ, P. 2021 Asymptotics of streamwise Reynolds stress in wall turbulence. *J. Fluid Mech.* **931**, A18.

MONKEWITZ, P.A., CHAUHAN, K.A. & NAGIB, H.M. 2007 Self-consistent high-Reynolds-number asymptotics for zero-pressure-gradient turbulent boundary layers. *Phys. Fluids* **19**, 115101.

MOSER, R.D., KIM, J. & MANSOUR, N.N. 1999 DNS of turbulent channel flow up to $Re_\tau = 590$. *Phys. Fluids* **11**, 943–945.

NAGIB, H.M., CHAUHAN, K.A. & MONKEWITZ, P.A. 2007 Approach to an asymptotic state for zero pressure gradient turbulent boundary layers. *Phil. Trans. R. Soc.* A **365**, 755–770.

ORLANDI, P. & LEONARDI, S. 2007 Technical Report for WALLTURB project. *Tech. Rep.* WT-071016-URS-1.

ÖRLÜ, R. 2009 Experimental studies in jet flows and zero pressure-gradient turbulent boundary layers. PhD thesis, KTH, Stockholm.

PANTON, R.L., LEE, M. & MOSER, R.D. 2017 Correlation of pressure fluctuations in turbulent wall layers. *Phys. Rev. Fluids* **2**, 094604.

PIROZZOLI, S., ROMERO, J., FATICA, M., VERZICCO, R. & ORLANDI, P. 2021 One-point statistics for turbulent pipe flow up to $Re_\tau \approx 6000$. *J. Fluid Mech.* **926**, A28.

SAMIE, M., MARUSIC, I., HUTCHINS, N., FU, M.K., FAN, Y., HULTMARK, M. & SMITS, A.J. 2018 Fully resolved measurements of turbulent boundary layer flows up to $Re_\tau = 20000$. *J. Fluid Mech.* **851**, 391–415.

SCHLATTER, P. & ÖRLÜ, R. 2010 Assessment of direct numerical simulation data of turbulent boundary layers. *J. Fluid Mech.* **659**, 116–126.

SCHLATTER, P., ÖRLÜ, R., LI, Q., BRETHOUWER, G., FRANSSON, J.H.M., JOHANSSON, A.V., ALFREDSSON, P.H. & HENNINGSON, D.S. 2009 Turbulent boundary layers up to $Re_\theta = 2500$ studied through simulation and experiment. *Phys. Fluids* **11**, 051702.

SILLERO, J.A., JIMENEZ, J. & MOSER, R. 2013 One-point statistics for turbulent wall-bounded flows at Reynolds numbers up to $\delta^+ = 2000$. *Phys. Fluids* **25**, 105102.

SKOTE, M. 2001 Studies of turbulent boundary layer flow through direct numerical simulation. PhD thesis, KTH, Stockholm.

SMITS, A.J., HULTMARK, M., LEE, M., PIROZZOLI, S. & WU, X.H. 2021 Reynolds stress scaling in the near-wall region of wall-bounded turbulence. *J. Fluid Mech.* **926**, A31.

SMITS, A.J., MCKEON, B.J. & MARUSIC, I. 2011 High-Reynolds number wall turbulence. *Annu. Rev. Fluid Mech.* **43**, 353–375.

SPALART, P.R. 1988 Direct simulation of a turbulent boundary layer up to $Re_\theta = 1410$. *J. Fluid Mech.* **187**, 61–98.

SREENIVASAN, K.R. 1989 The turbulent boundary layer. In *Frontiers in Experimental Fluid Mechanics* (ed. M. Gad-el-Hak), pp. 159–209. Springer.

TARDU, S. 2017 Near wall dissipation revisited. *Intl J. Heat Fluid Flow* **67**, 104–115.

TOWNSEND, A.A. 1956 *The Structure of Turbulent Shear Flow*. Cambridge University Press.

VALLIKIVI, M., GANAPATHISUBRAMANI, B. & SMITS, A.J. 2015 Spectral scaling in boundary layers and pipes at very high Reynolds numbers. *J. Fluid Mech.* **771**, 303–326.

VINCENTI, P., KLEWICKI, J., MORRILL-WINTER, C., WHITE, C.M. & WOSNIK, M. 2013 Streamwise velocity statistics in turbulent boundary layers that spatially develop to high Reynolds number. *Exp. Fluids* **54**, 1629.

WILCOX, D.C. 2006 *Turbulence Modeling for CFD*. DCW Industries.

WILLERT, C., SORIA, J., STANISLAS, M., KLINNER, J., AMILI, O., EISFELDER, M., CUVIER, C., BELLANI, G., FIORINI, T. & TALAMELLI, A. 2017 Near-wall statistics of a turbulent pipe flow at shear Reynolds numbers up to 40 000. *J. Fluid Mech.* **826**, R5.

WU, X.H. & MOIN, P. 2008 Direct numerical simulation on the mean velocity characteristics in turbulent pipe flow. *J. Fluid Mech.* **608**, 5–41.

YAMAMOTO, Y. & TSUJI, Y. 2018 Numerical evidence of logarithmic regions in channel flow at $Re_\tau = 8000$. *Phys. Rev. Fluids* **3**, 012602.

YANG, X.I.A., HONG, J., LEE, M. & HUANG, X.L.D. 2021 Grid resolution requirement for resolving rare and high intensity wall-shear stress events in direct numerical simulations. *Phys. Rev. Fluids* **6**, 054603.

YANG, X.I.A. & LOZANO-DURÁN, A. 2017 A multifractal model for the momentum transfer process in wall-bounded flows. *J. Fluid Mech.* **824**, R2.

YAO, J., CHEN, X. & HUSSAIN, F. 2019 Reynolds number effect on drag control via spanwise wall oscillation in turbulent channel flows. *Phys. Fluids* **31**, 085108.

YEUNG, P.K., SREENIVASAN, K.R. & POPE, S.B. 2018 Effects of finite spatial and temporal resolution in direct numerical simulations of incompressible isotropic turbulence. *Phys. Rev. Fluids* **3**, 064603.